Temperature-Sensitive Contact Modes Allosterically Gate TRPV3

Daniel Burns[2], Vincenzo Venditti[1,2], Davit A Potoyan[1,2]

1. Department of Chemistry, Iowa State University, Ames IA 50011
2. Roy J. Carver Department of Biochemistry, Biophysics and Molecular Biology

Abstract

TRPV Ion channels are sophisticated molecular sensors designed to respond to distinct temperature thresholds. The recent surge in cryo-em structures has provided numerous insights into the structural rearrangements accompanying their opening and closing; however, the molecular mechanisms by which TRPV channels establish precise and robust temperature sensing remain elusive. In this work we employ molecular simulations, multi-ensemble contact analysis, graph theory, and machine learning techniques to reveal the temperature-sensitive residue-residue interactions driving allostery in TRPV3. We find that groups of residues exhibiting similar temperature-dependent contact frequency profiles cluster at specific regions of the channel. The dominant mode clusters on the ankyrin repeat domain and displays a linear melting trend, while others display non-linear and sometimes increasing contact-frequency trends. These modes describe the residue-level temperature response patterns that underlie the channel's functional dynamics. With network analysis, we show that the community structure of the channel changes with temperature, providing a detailed description of temperature-dependent domain coupling. We also find a network of high centrality contacts that connects distant regions of the protomer to a point directly adjacent to the gate, serving as a means for the temperature-sensitive contact modes to allosterically regulate channel gating. Using a random forest model, we show that the contact states of specific temperature-sensitive modes are indeed predictive of the channel gate's state. Supporting the physical validity of these modes and networks are several residues identified with our analyses that are reported in literature to be functionally critical. Our results offer a model for thermo-TRP channel function and demonstrate the utility of temperature-sensitive contact analysis.

Introduction

Transient Receptor Potential Vanilloid 3 (TRPV3) is a tetrameric divalent cation channel and member of the ion channel family responsible for the molecular basis of temperature sensation[1,2]. TRPV3 is expressed in skin keratinocytes [3] and is associated with Olmsted Syndrome, atopic dermatitis, and hair growth defects [4–7]. Structurally, it is characterized by a large intracellular skirt composed of ankyrin repeat domains (ARDs) (Fig. 1). Each subunit interfaces with the adjacent protomer's ARD via an inter-protomer coupling domain (IPCD) composed of antiparallel beta strands. A transmembrane voltage sensing like domain (VSLD) and pore domain interface with adjacent subunits within the membrane. At the junction between the transmembrane and ARD domains, the namesake TRP helix lies horizontally along the inner membrane, above the so-called Helix Turn Helix (HTH). Both the N and C terminal tails are disordered and almost entirely absent from available structures, however in the structures where they are resolved they exhibit different conformations depending on the channel's state[8–10]

The pore itself is characterized by a central cavity between an extracellular selectivity filter and lower gate. Upon activation, the gate radius widens by approximately 1.5 angstroms [8] to allow passage of Ca2+ ions to the intracellular space. In order to function, TRPV3 has an additional sensitization requirement where the channel must first be exposed to temperatures exceeding 50°C before it can be activated by temperatures above 30°C [8,9,11–14]. The mechanism translating temperature increase to gate expansion in thermo-TRP channels is not well understood despite a number of reported structural changes that coincide with the open gate [8,9,15–18].The identification of temperature-sensing regions and an explanation of how these regions coordinate their dynamics to control gating within a precise temperature range are of fundamental importance for understanding the design principles of temperature-sensing ion channels.

Recently, cryo-EM structures have provided a coarse description of the channel's dynamics composed of closed, sensitized, and open states, but high-resolution molecular dynamics simulations of thermo-TRP channels are few [8,19–24]. Moreover, computational studies have yet to reveal the underlying principle of thermo-TRP regulation. In this work we employ atomistic simulations, contact network analysis and machine learning techniques to provide a mechanistic explanation for allosteric regulation of TRPV3 and identify specific regions and residues implicated in temperature sensing.

Starting from an initially closed structure of TRPV3 we use Hamiltonian Replica Exchange Molecular Dynamics (HREMD) to sample the conformational ensembles of the channel across a wide range of temperatures. Then, utilizing all-atom contact calculations, we identify the most temperature-sensitive inter-residue contacts via Principal Component Analysis (PCA)[25]. The application of PCA segregates all of the pairwise interactions into distinct modes describing their temperature-dependent behavior. These modes are centered on important regions of the channel and can be reconciled with experimental results as the residues defining them overlap with mutational and allosteric hot spots.

To identify allosteric pathways that couple domains and communicate sensation of heat across the structure, we employ network analysis methods, using contact frequencies as edge weights.

Finally we use the instantaneous contact records and gate radius measurements in a random forest model to identify which temperature-sensitive contact modes best inform on the expansion of the channel's gate. Our results identify many important interactions that are supported by previous experimental research and offer a model by which thermosensitive ion channels can exhibit activity precisely tuned to temperature.

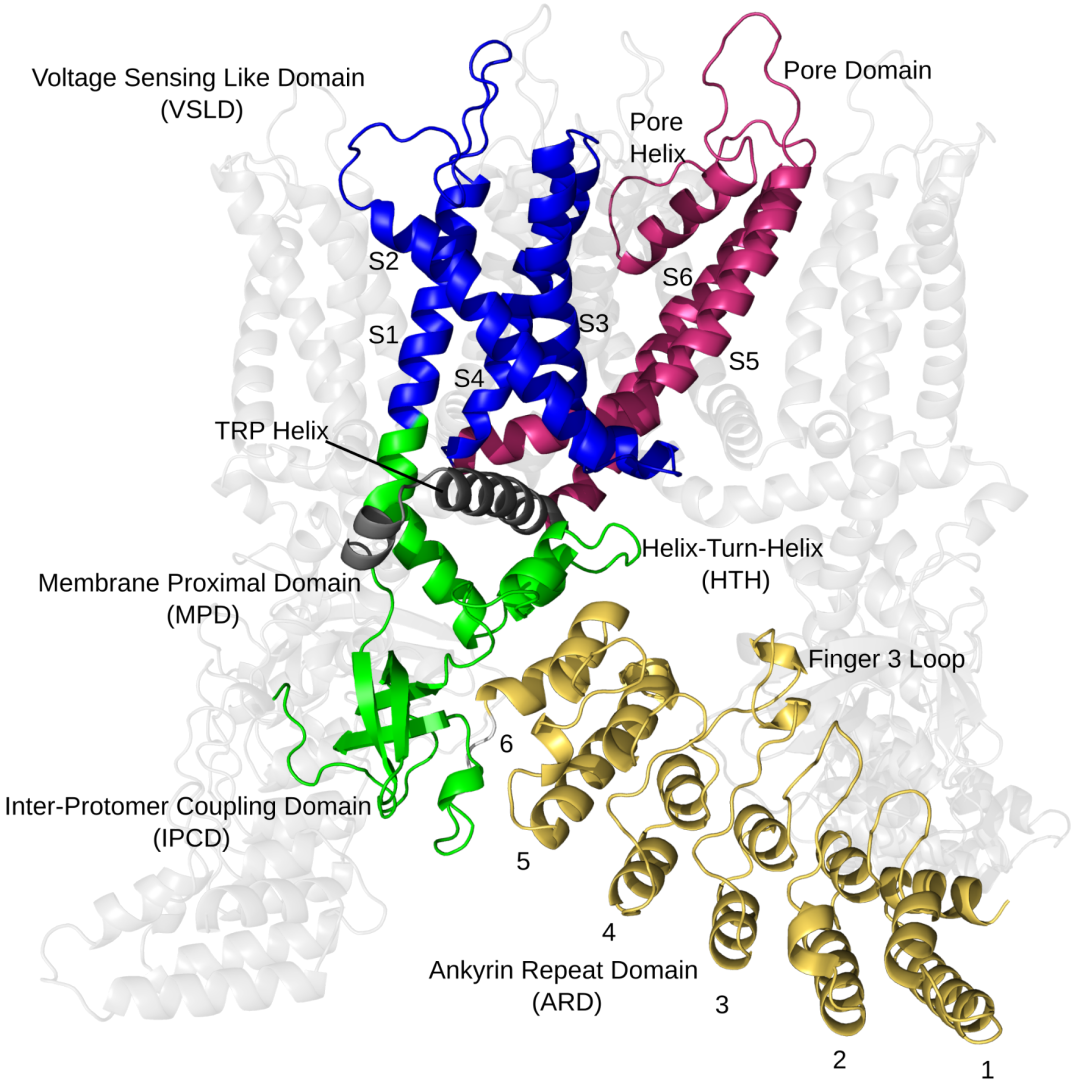

Figure 1. TRPV3 protomer domain structure. Shown is a single protomer in relation to two adjacent protomers (light gray) with opposing 4th protomer hidden. The green region closely matches the Membrane Proximal Domain (MPD) as identified by Qin and colleagues[26] and includes the subdomains of the HTH and Inter-Protomer Coupling Domain (IPCD) composed of beta strands which contact the adjacent protomer's ARD and Finger 3 Loop.

Results

Temperature sensitive contacts

Thermo-TRP channels allosterically respond to temperature changes with rearrangements that expand their pore and allow ions to diffuse through. Experimental structures provide the endpoints of this process but leave out the mechanistic details of intermediate steps. To investigate the continuous space between the endpoints, we sampled the equilibrium inter-residue contacts by simulating TRPV3 across 28 effective temperatures spanning the sub-activation, activation, and above physiological range. From these we calculated all of the inter-residue contact frequencies.

By applying PCA on the temperature-dependent contact frequency data [25] we extract principal components which describe the ion channel's collective contact making and breaking responses to temperature. Each contact has a unique loading score (eigenvector component) describing the contact's contribution to the variance described by the PC. Here the normalized loading score is used to rank a contact's temperature-sensitivity within different PC trends, or "modes". These modes can reveal where temperature-sensing function is localized as well as allosteric connections since the loading scores within a PC are a measure of correlation between contact responses.

The PC1 mode accounts for nearly 40% of the variance in the contact frequency data (fig 2A) and captures the expected melting trend where contact frequency decreases with increasing temperature (Fig 2B red). PC2 accounts for roughly 12% of the explained variance and describes a less intuitive consequence of increased temperature: an increase in contact frequency for many of its highest ranking contacts (Fig. 2B blue, see Fig. S1 for individual contacts). The subsequent PCs describe trends that oscillate within progressively narrower temperature and frequency ranges. By PCs 5-7 a local maximum amplitude develops around the sensitization temperature of TRPV3 (fig 2B vertical dashed bar).

Structurally Clustered Modes Identify Temperature Sensing Regions

Structural clustering is evident among the top ranking contacts of the first seven PCs (Figure 2C). Many of the most sensitive contacts in these clusters have experimental significance that we note here. From thousands of contacts, we consider only the 99.85th percentile of the loading scores (18 contacts) on each PC to represent the highly temperature-sensitive interactions(Fig S2). This percentile captures the upper half of the narrow range of rapidly decaying loading scores (Fig S3). Thus the following correspondences between these contacts and previously published data is remarkable.

Regarding the thermodynamics of TRP gating, Yao et al. showed that ankyrin repeats 5 and 6 were responsible for the activation enthalpy differences between TRPV1 and TRPV2 [26]. This observation can easily be explained in the context of TRPV3 by the densely clustered PC1 melting trend that spreads out from ankyrin repeat 5 (Fig 2C red). Indeed, PC1's prominent role

on the ARD becomes more apparent when expanding the range of depicted contacts' loading scores(Fig. S4).

In contrast to PC1, most of PC2's top contacts display increasing frequency with temperature (across the physiological range). An expanded set of PC2 contacts clusters heavily around the middle of the protomer, overlapping with PC1 on the upper ARD, surrounding the IPCD, and extending into the VSLD (Fig S5). In the context of the first 7 PCs', PC2 best describes a dispersed set of generally order promoting interactions (fig 2 C blue, solid lines . Perhaps the most notable correspondence with experimental work is the overall highest ranked PC2 contact between T411 on the HTH and L508 on the S2-S3 linker. T411 is at (or in terms of substitutions, "adjacent to") the position identified by Liu and Qin[11] where an insertion of a cognate residue from TRPV1 eliminates the use-dependent sensitization of TRPV3. In fact, both residues of this contact carry significance as a recent study showed L508 to be the most important residue in binding the allosteric activator carvacrol [27]. PC2's 9th ranked contact involving Y564 and F522, which connects the S4 and S3 helices, also has experimental significance. When mutated to alanine, Y564A enhances binding of the allosteric activator 2-APB [18,28], a ligand which has played an important role in TRPV3 studies.

PC3 (Fig. 2C green) describes a mode with sparsely distributed contacts localized mostly to the upper ARD and lower transmembrane region . Though structurally isolated, PC3's 5th ranked and most notable experimentally relevant contact is S5-Pore helix linker between N647 and C619, as an N647Y mutation was shown to eliminate activity[29]. PC4 clusters on both the extracellular loops and around the IPCD (Fig. 2C purple). Because these regions are so distant, it's likely that PC4 encompasses the dynamics of two structurally independent modes that exhibit similar temperature-dependent contact frequency profiles. Notable on PC4 is a highly sensitive contact in the finger 3 loop near the IPCD, involving F249, which was shown to alter the channel's sensitivity to chemical stimulation when mutated[30].

PC5 is the dominant mode of the extracellular VSLD loops (Fig. 2C dark grey) where most of the contacts display a subtle increase in frequency within the physiological temperature range. Residues Y540 and R487 are involved in the 7th and 8th most temperature-sensitive contacts on this PC and both involved in a binding site of the allosteric activator 2-APB [28]. PC6 clusters along the TRP helix/S6 bend (Fig. 2C magenta) just below the gate itself, precisely where structural changes are associated with gating [28] . Most notable on PC6 is the 4th ranked, functionally critical residue, T680. Mutating T680 to alanine to break its hydrogen bond with D586 abrogated activity in an experimental TRPV3 construct [15]. Lastly, PC 7 clusters heavily around the IPCD and adjacent finger 3 loop(Fig 2C gold). Several of the residues in PC7's highly temperature-sensitive contacts surrounding the IPCD are involved in the state-dependent exchange of the N and C terminal tails[8] including R226, N273, W742, K743, and H745 (Fig/Table. S2). Among the highest ranking PC7 contacts (rank 8), W742 was shown to substantially reduce channel activity upon mutation to alanine [9].

The lower eigenvalue PC projections (4-7) show a local maximum (Fig 2B vertical dashed line) in the temperature range where physiological activation of TRPV3 occurs [11]. Since PC6 is clustered immediately by the gate, we found it likely that the overlapping activation maximum was not merely a coincidence. The other PC clusters, however, are quite distant from

the gate, prompting us to investigate a means of communication between them and the gate.

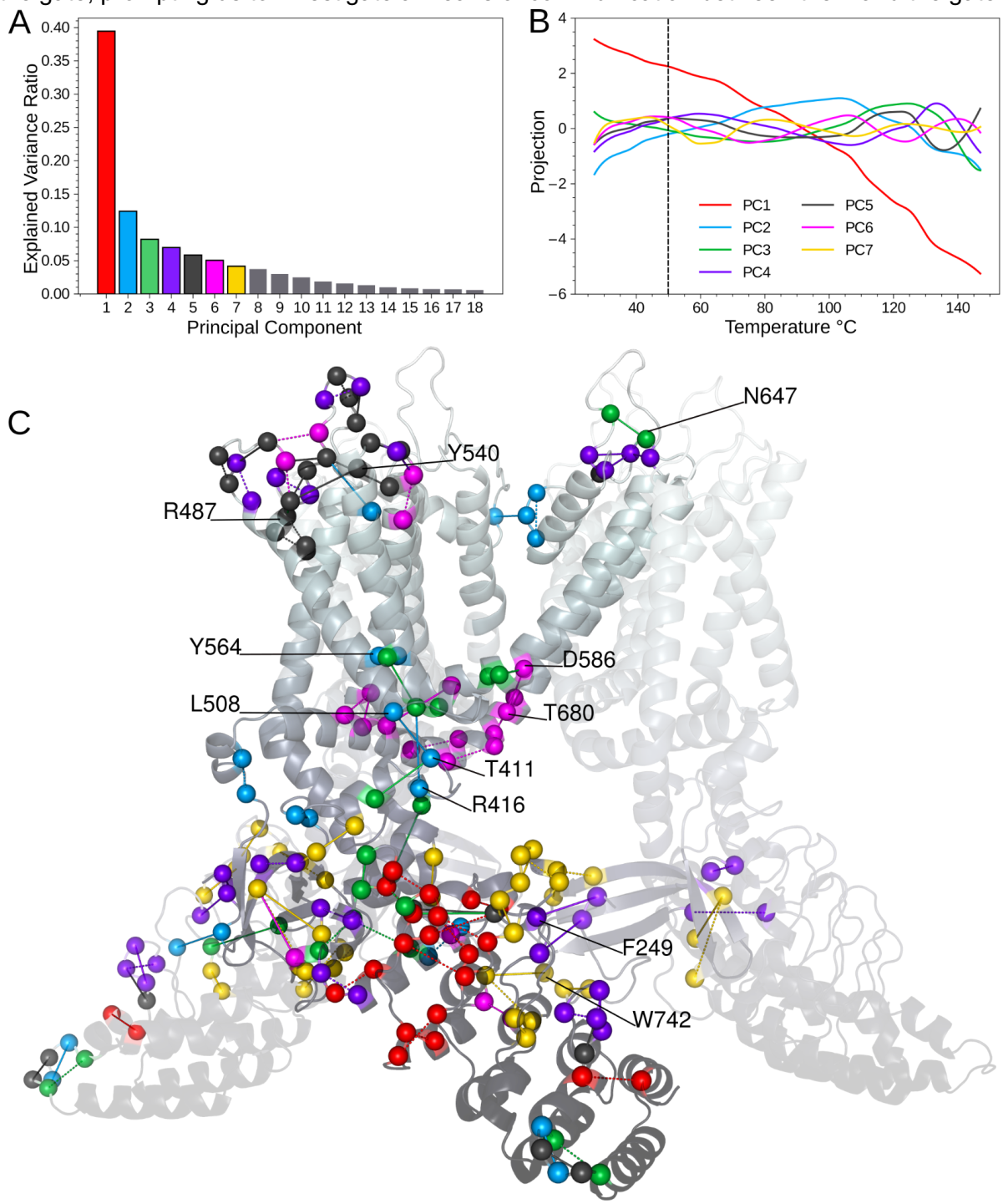

Figure 2. Temperature-sensitive contact analysis of TRPV3. **A.** Explained variance of the contact frequency principal components. **B.** PC projections showing the general trend in contact frequencies across temperature for the first 7 PCs. See figure S1 for plots of individual contact frequencies. **C.** TRPV3 structure (rear protomer not depicted) showing the most temperature-sensitive contacts (99.85th percentile) from each of the top 7 PCs. The overall top ranking contact for the given residue is depicted and colored according to the PC on which it has the

highest loading score following the same PC color scheme in 5A/B. Solid lines indicate contacts that tend to increase in frequency within the physiological range and dashed lines indicate contacts that tend to decrease in frequency (based on linear fits) in the physiological range. The contacts surrounding the IPCD are duplicated on either side of the central protomer and those extending down to the distal end of the ARD are duplicated on the left protomer to reflect the influence a protomer experiences from the neighboring subunits. Allosterically important residues discussed in text are indicated.

Allosteric networks couple domain motions in TRPV3

Though debate regarding the presence of a single vs distributed temperature-sensing module has not been fully resolved, experiments on several TRP channels suggest that a single domain is responsible for determining the gross activation temperature range [31],[26,32] with the coordination of multiple domains necessary for gate activation and fine-tuned temperature specificity[29,33,34]. A prevalent view is that these multiple regions respond by enhancing inter-domain 'coupling'[9,35–38]. Here we perform network analysis to investigate the temperature-dependent domain coupling by applying the contact frequencies as network edge weights using data from the 27°C (below activation, lowest temperature simulation) and 54°C (>50°C, initial sensitization) [18] simulations.

Network analysis techniques have been used to identify communication pathways in proteins as well as communities of residues that comprise functional domains [39–43] and can offer a detailed description of this coupling. Indeed, similar analysis has been applied to coarse-grain simulations of TRPV1 [19].

Network Community Structure

A network can be partitioned into communities with the Girvan-Newman [44]algorithm by calculating all of the shortest paths (based on contact frequency edge weights) between nodes, removing the highest betweenness-centrality[45] edge and then repeating this process until the network has been broken up into a pre-defined number of communities with no more edges connecting them to one another.

We initially partitioned the TRPV3 protomer into 5 communities which returned a community structure that corresponded very closely to the accepted domain structure; however by specifying 6 communities we discovered that the community structure displayed a visible correspondence with the dynamics and temperature-sensitive contacts of the ARD. Specifically, a clean division of the ARD community structure occurs at the region in which both our simulations and earlier published coarse-grained simulations on TRPV1[19], as well as structural data [8,18,28] show large motions develop on the first repeats . This boundary of the two ARD communities is also conspicuously located directly under the disordered tail binding site and IPCD (fig 3A)[46], adjacent to the finger 3 loop [30],and on the edge of the PC1 contact cluster.

Community Coupling

Since temperature is proposed to enhance coupling between domains, leading to channel activation [35], we expected the community structure to change with temperature. While the

ARD maintains almost identical community structure between temperatures (Fig. 3A purple and gold communities), this is not the case for other critical regions of the protein. The most apparent illustration of altered domain coupling is seen in the upper S1 and S4 helices and the entirety of the S2 and S3 helices. These areas form a distinct community at low temperature (Fig. 3A 27 °C, grey community) but merge with the lower VSLD and TRP community at high temperature (Fig. 3A 54 °C blue community).

Importantly the HTH also exhibits a significant change in its community structure (Fig 3A close-ups), albeit a subtle one considering that the HTH is composed of few residues relative to the channel's size. At low temperature the HTH participates largely in the same community as the IPCD (Fig 3A red community), which together with the lower S1 roughly corresponds to the Membrane Proximal Domain identified in Yao et al.,2011 [26]. The HTH is nonetheless connected to other communities including those of the S3-S4 kink (via T411) (grey community at 27 °C), TRP helix (blue community), and ARD (gold community), reflecting its central position in the structure's network. At high temperature, however, the HTH community structure is noticeably altered and almost entirely coupled to the VSLD (blue) community.

The smallest community at high temperature occurs on the pre-S5 helix and adjacent S6-TRP bend (54 °C grey community). This region overlaps with the cluster of PC6 contacts (Fig 2C magenta) and region where state-dependent helix unwinding occurs[28]. The change in contact frequencies, as a consequence of temperature increase, reorganizes the interaction network and enhances coupling between the intra and extracellular domains.

Edge Betweenness-Centrality and Allosteric Pathways

The TRPV3 selectivity filter is constitutively active and apparently not under allosteric regulation of other domains [36]. Because the gate around residue I674 is the only other constriction point within the pore, allosterically important dynamics must somehow be integrated here to precisely regulate a ~1.5 angstrom expansion. To investigate the pathways by which the distant domains can communicate with the gate, we calculated edge betweenness-centrality values using contact frequencies from the 54°C simulation (where a network associated with the sensitized state should develop) as edge weights. Figure 3B shows the top central edges (Fig. S6, left of vertical red cutoff bar) on the protomer structure with clear pathways running from the distal region of the ARD through the HTH and branching into the VSLD and pore domain. Surprisingly, despite the pore domain's relative isolation within the context of a single protomer, multiple pathways from distant regions converge in the S5 helix, directly adjacent to the gate residue of I674 (A closeup of the transmembrane region's edges is available in figure S7).

Several observations support that this "allosteric skeleton" includes physically real communication pathways as ligand binding sites and function-affecting mutation positions are among the residues defining the highest 30 betweenness-centrality edges. For instance, T636's contact with Y594 is the primary edge between the Pore and S5 helices and is directly adjacent to the S6 pi bulge [47]. Mutating T636 to serine resulted in a hyperactive mutant [48] and this same position is known to be a binding site for the inhibitor scutellarin [49].

The interaction between H426 and R693 is a central edge on the most direct path connecting the IPC domain and the TRP helix. H426 binds the agonist 2-APB [50] and both residues participate in binding the allosteric inhibitor Osthole [46]. The functionally critical

contact between T680 and D586 (mentioned above) is both a top temperature-sensitive contact and highly central edge suggesting it is of particular allosteric importance [15]. The contact between R416 and D519 connects the HTH to VSLD and is one of the only other contacts that is both highly temperature-sensitive and a highly central edge.

Qin and colleagues [11,51] have shown the large impact of mutations on this region and given that the HTH is the most direct route connecting a protomer's ARD to the transmembrane domain, this contact and and the aforementioned T411-L508 are likely critical for domain coupling as they both increase in frequency with temperature.

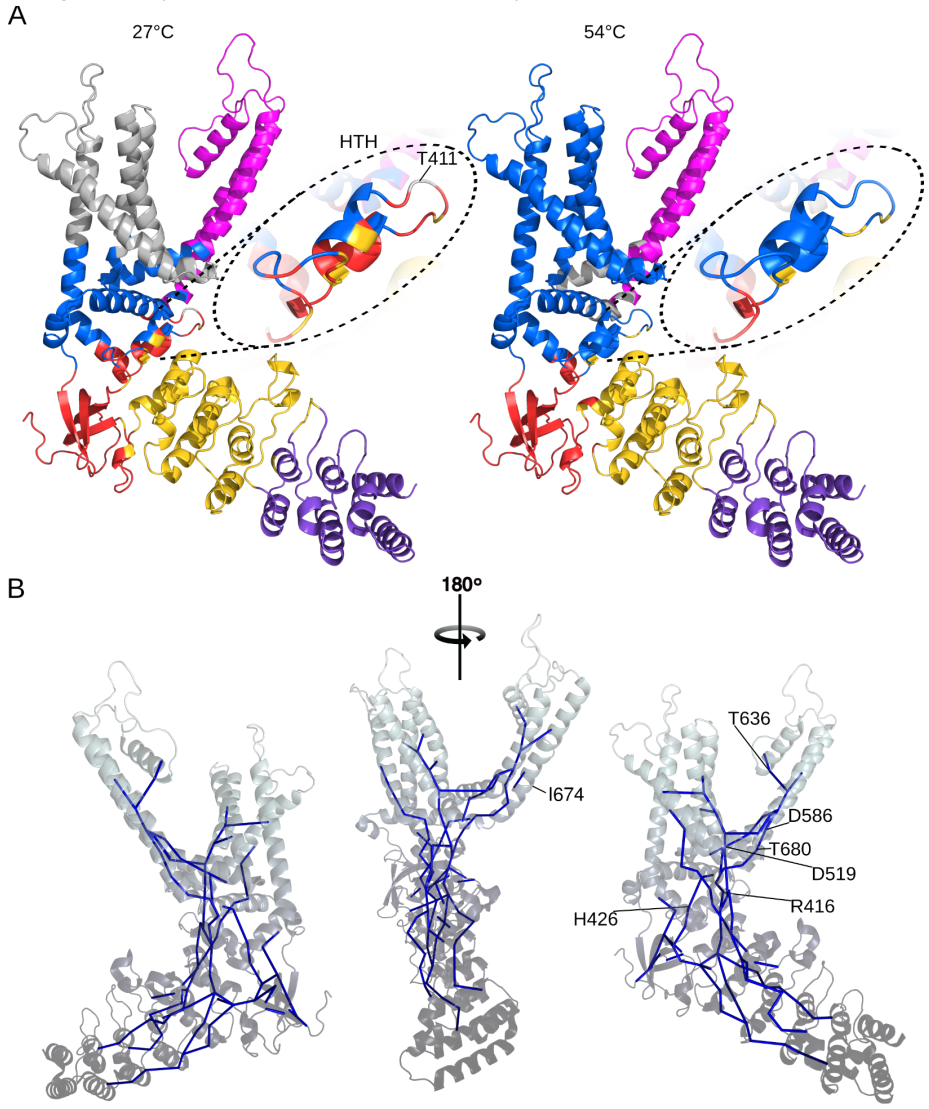

Figure 3. Network analysis of a TRPV3 protomer based on average contact frequency edge weights. **A.** Left: 6 communities constructed from the 27°C simulation contact frequencies. T411 is indicated to highlight its unique community participation among the HTH (close-up) residues. Right: 6 communities constructed from the 54°C (activation temperature) contact frequencies, displaying a notable change in community structure in the HTH and VSLD domain compared to

27 °C. **B.** 180° rotation of a protomer showing the top 86 highest betweenness-centrality edges constructed from the 54°C simulation's contact frequencies. Residues defining these edges have been noted based on their significance in literature (R416 because we remark on it).

The motions sampled by the TRPV3 protomer

The contact frequency PCs and networks do not directly inform on the 3-dimensional motions that the channel samples. Since cryo-em structures confirm that distributed conformational changes correlate to the state of the gate, we sought to relate the channel motions to the contact modes. To this end we performed PCA on the protomers' Cartesian coordinates from the 54 °C trajectory and extracted the endpoints of the largest motions from the first 6 PCs (Fig. 4) which describe from 5 to 20% of the variance (50% total) (Fig. S8).

The fact that the large bending and twisting motions of the ARD seen on Cartesian PCs 1 and 2 originate next to the contact PC1 cluster suggests that these dynamics And contacts are related. The melting of contact PC1 apparently creates a "hinge" region on the upper ARD, allowing the lower ARD to swing. Cartesian PC5 shows the HTH, TRP helix and S3-S4 bend compressing together at the (blue) end of the concerted motion, in line with the domain coupling seen in the high temperature community. Contact PC2 is the natural basis for this motion as it describes strongly increasing contact frequencies here.

Notable also is the correlation between the extracellular loop motions (particularly those on the VSLD linkers) and the motions of the transmembrane helices. The extracellular loops here are dominated by contact PCs 4 and 5 making their interactions the likeliest source of these upper transmembrane dynamics. The subtle IPCD motions on Cartesian PCs 3, 5, and 6 are most attributable to the interactions described by contact PCs 4 and 7 as they surround the IPCD. Interestingly, the pore domain exhibits its most apparent motions on these PCs as well.

The gating of the channel is most directly a function of conformational dynamics, but the dynamics themselves are a function of the strengths and temperature-sensitivities of the underlying residue interactions. To move towards a precise, residue-level description of the temperature-dependent regulation of TRPV3 we sought to connect the temperature-sensitive contact modes to gate dynamics.

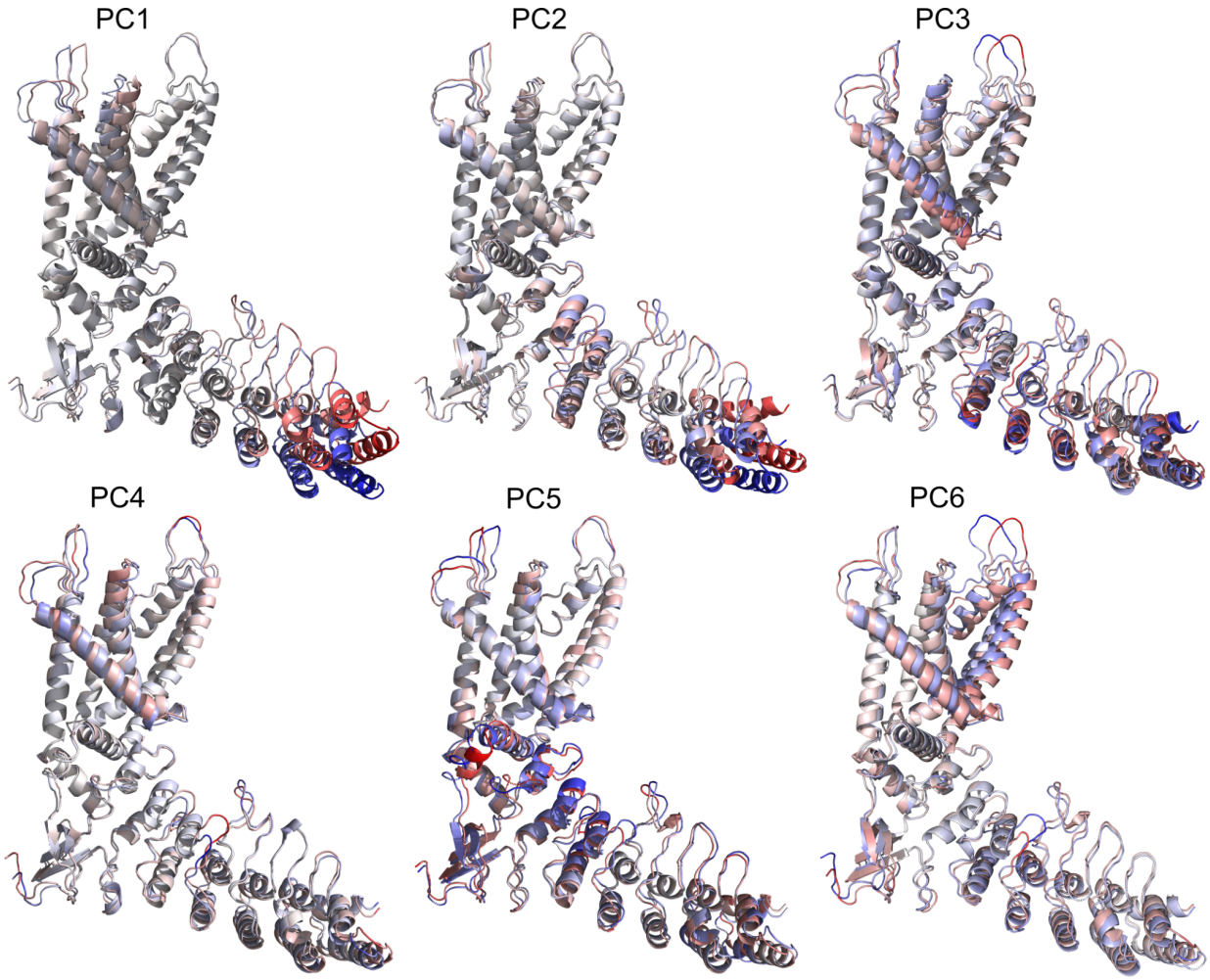

Figure 4. Extremes of the protomer structures (red or blue) extracted from the corresponding PC trajectory projections and colored according to regions of maximum displacement.

Allosteric Gating

To test whether the contact frequency modes are indeed coupled to the gate, we turned to supervised shallow machine learning, specifically a random forest, as it can pull important features out of the inherently noisy biomolecular interaction space and provide readily interpretable model coefficients.

Here we utilized the Hole [52] calculation to determine the gate radius (Fig 5 A & B) and construct binary labels to classify the gate at each frame in the trajectory. We identified an "expanded" gate as a minimum radius greater than 1 angstrom (Fig 5C) (corresponding to the radius of a Ca^{2+} ion [53]) and calculated the number of frames at each temperature where the radius was above the cutoff. Figure 5D shows that the P(expanded gate) (number of frames where gate radius > 1 Å/ total frames) trends up from baseline near the physiological activation temperature to a local maximum at sensitization temperature before returning to baseline (only spiking again after ~100°C). Interestingly, the contact PC 5 and 6 projections appear similar to

the expanded gate trend in the physiological temperature range, having respective Pearson correlation coefficients of 0.89 and 0.91 between 27° to 62°C (Lowest sub-activation simulation temperature to just above maximum temperature recorded in Liu & Qin 2011 [11]) .

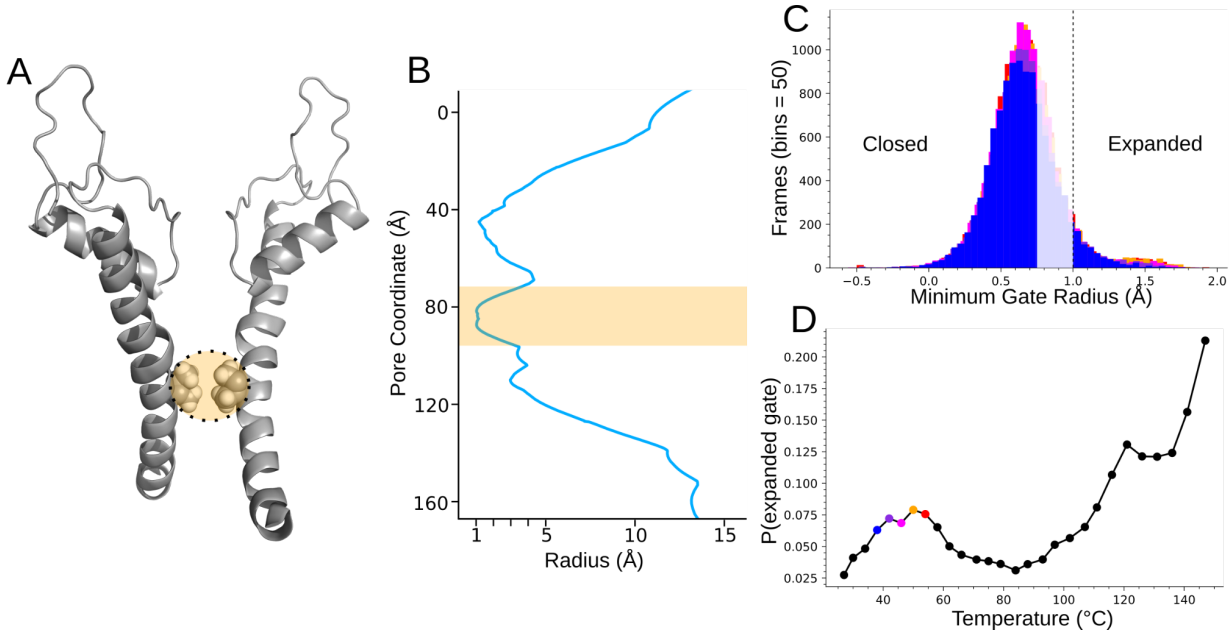

Figure 5. Gate measurement. **A.** Two opposing S6 helices defining the pore region of TRPV3 with I674 gate residues highlighted. **B.** Example Hole analysis pore profile with the gate region highlighted. The narrow central region of the profile corresponds to the actual pore. The minimum value in the highlighted region was used to define the state of the gate for the random forest model. **C.** Overlapping histograms of the gate radius from the five simulations used to construct the random forest input data. The faded region of the histogram represents the gate data that was not included in the random forest in order to discretize the expanded and closed states. Expanded gate state occurs to the right of the vertical dashed line. **D.** Probability of the expanded gate vs. temperature showing a local maximum around the physiological activation temperature. Colored dots indicate the simulations used in the random forest.

The input data for our random forest model was the binary state of each contact at each frame of the simulations. With this, we trained a random forest to identify an expanded gate based on the contact states of a TRPV3 protomer. The purpose of building this model was to extract the contacts to which the model assigned high feature importance, revealing the interactions and corresponding modes that influence gate expansion.

Fitting several models with between 75 and 80% accuracy at predicting the expanded channel state, we determined on which PC each of the top 100 important contacts have their highest loading score. Figure S9 shows that beyond the first 100 contacts, the feature importance drops to essentially 0 and the remaining contacts become uninformative. PC7 and PC2 proved to be the dominant modes, followed closely by PCs 5 and 6 , whereas PCs 1,3, and 4 are underrepresented (Fig 6A, individual model results in Fig S10). We took the intersection of

the top 100 features from the two models with the most generally fit parameters which returned 83 shared contacts. The structure depicting the high feature importance contacts (Fig 6C) is reminiscent of the conformational wave which accompanies state transitions proposed by Nadezhdin and coworkers[8]. Figure 6B indicates that the contacts most predictive of the expanded gate occur not only primarily amongst the lower eigenvalue modes but also in the middle of the temperature sensitivity scale. Although structural clustering of contact modes is less apparent than when considering only the top loading scores, the distribution of loading scores and PCs among the predictive contacts (Fig 6B) illustrates the channel function's reliance on many interdependent dynamics. Nevertheless PC1 clusters heavily on the ARD, PC2 on the HTH, and PC7 around the IPCD.

In addition to it having the highest population of top feature important contacts, PC7's high ranking temperature-sensitive contacts show contact frequency changes of similar magnitude to P(expanded gate) in the activation temperature range (Fig S1). The functional significance of the PC7 IPCD clustering in both feature importance and temperature-sensitivity is supported not only by the state-dependent exchange of the disordered terminal tails around the IPCD [8,9] but also by a 2003 study showing that the distal end of the TRPV1 C-terminal tail confers thermal specificity [34]. The small magnitude of P(expanded gate) appears to recapitulate the reduction in heat-evoked currents seen with their 72 aa truncation, given that the simulated structure lacks a similar number of C-terminal residues.

Interestingly, the extracellular VSLD loops, where the most dominant temperature-sensitive modes are PCs 4 and 5, show several PC7 contacts among the high feature importances. Although some of these residues have higher scoring contacts with other partners on higher eigenvalue PCs, their secondary interactions manifest the same mode that characterizes the IPCD. These PC7 contacts involve residues farther down the S2, 3, and 4 helices than any of the other high feature importance VSLD contacts, likely exerting more influence on the helix structure deeper in the membrane (and closer to the gate) than the interactions restricted to the solvated portions of the loops.

Many of these high feature importance contacts are also the top ranking temperature-sensitive contacts including the overall highest ranking contacts on PCs 1,2,6 and 7. Seven of the top 11 temperature-sensitive contacts appear from PC7; more highest ranking contacts than any other PC. Of the functionally critical residues identified in literature, we find that the top ranking PC2 contact involving T411 and L508, the 4th ranked PC6 contact between D586 and T680, the 2-APB binding residues Y540 and R487, and contacts with F249 on the finger 3 loop adjacent to the IPCD, to have states that are highly predictive of the expanded gate. Feature important contacts involving D586, Y540 and R487 also exhibit the PC7 mode despite occurring in places distant from the IPCD.

Not only do PCs 2 and 5-7 exhibit more of the top feature importances than PCs 1,3, and 4, they also contain the contacts with the highest feature importance values. The 3 highest feature importances overall are found at the distal end of the ARD, the finger 3 loop, and the IPCD (Fig 6C Q227-K184, N251-Y254, R729-R371), suggesting that a dynamic originating around the IPCD regulates the final step in gating.

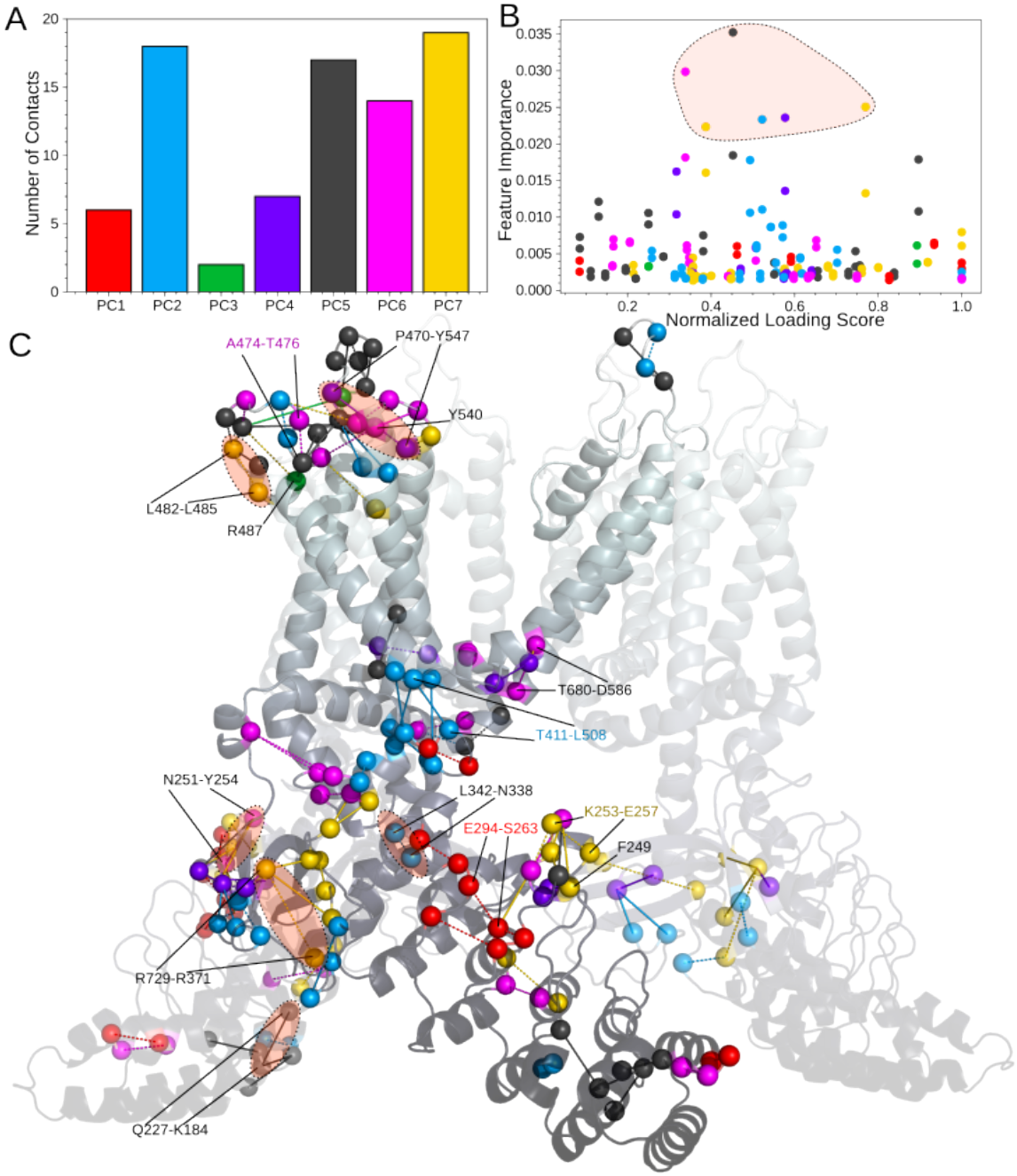
A
Number of Contacts
0
5
10
15
20
PC1
PC2
PC3
PC4
PC5
PC6
PC7
B
Feature Importance
0.000
0.005
0.010
0.015
0.020
0.025
0.030
0.035
0.2
0.4
0.6
0.8
1.0
Normalized Loading Score
C
A474-T476
P470-Y547
Y540
L482-L485
R487
T680-D586
T411-L508
N251-Y254
L342-N338
K253-E257
E294-S263
F249
R729-R371
Q227-K184

Figure 6. Random forest feature importance analysis. **A**. The counts of each PC's contacts that occurred in the intersection of the 2 random forests' top 100 feature important contacts. **B**. Feature importance vs. loading score (rank) for top contacts in the intersection of the two random forest models. The contacts were assigned the PC on which they have their highest loading score and colored accordingly. The pairs of vertically aligned dots appear because feature importance values from both random forests are shown. The colored region outlined with the dashed line indicates the highest feature importance contacts that are highlighted similarly on the structure. **E**. Depiction of the intersection of the 2 random forests' highest feature importance contacts on the TRPV3 protomer with the contacts on the ARD and surrounding the IPCD duplicated to illustrate their influence from the adjacent subunits. For residues involved in several contacts exhibiting different modes, the residue is colored according to the contact having the highest feature importance in either of the 2 models. Solid lines indicate contacts that increase in frequency within the physiological range and dashed lines indicate decreasing frequency (based on linear fits) in the physiological range. High feature importance residues with experimental significance are noted as well as the most temperature-sensitive contacts on PCs 1,2,6, and 7 which are identified with correspondingly colored text. The 6 highest feature importance interactions are highlighted with transparent ovals corresponding to the colored region in B. Rear protomer not shown.

DISCUSSION

Despite decades of work on temperature sensing ion channels, a detailed description of how they sense distinct temperature thresholds and allosterically regulate their pores in response remains lacking. In this work we employed molecular simulations, temperature-sensitive contact analysis, graph theory, and machine learning to reveal details of allosteric regulation in TRPV3.

We used temperature-sensitive contact analysis to decompose the channel's temperature response into several structurally localized, collective residue interaction modes that underlie the channel's dynamics. Our network analyses provide a straightforward description of temperature-enhanced domain coupling and reveal a network of high centrality contacts that connects distant regions of the protomer to a point directly adjacent to the gate. The random forest model reveals correlations between specific temperature-sensitive contact modes and gate expansion, and points to the region of the channel from which the final step in gating is regulated.

The results offer a model for TRPV3 function that accounts for published observations and suggests a means of specific temperature tuning for other TRP channels. First, the overwhelming majority of the melting described by contact PC1 develops adjacent to the dynamic lower ARD, suggesting that it influences these motions. The ARD's motions transmit force through the allosteric network, likely contributing to gate activation. Indeed, a precedent for this mechanism exists in another TRP member, the NOMPC mechanotransduction channel, whose large ankyrin repeats convey force that underlies its gating[54]. The PC1 mode also partly explains the channel's change in heat capacity related to activation which requires the exposure of roughly 20 nonpolar residues to solvent [55,56]. The entropic payment for the increased local order described by the lower eigenvalue PCs can also be attributed to it.

Moreover, the ARD is known to be the primary temperature sensor for (rattlesnake) TRPA1 [32] and, given the high explained variance of PC1, it appears to serve the same role here. Thus the PC1 mode promotes disorder which evolves with temperature to a point where numerous distributed interactions form, following the progressively more subtle PC trends, before the probability of channel opening is high enough to be physiologically relevant.

While the ARD dynamics influence the channel from the intracellular side, the VSLD loops influence it from the extracellular side. The structural clustering of the PC4 and PC5 modes make them the most apparent source of the subtle bends and shifts of the VSLD helices which must sterically influence the gate, and based on their projected trends, their interactions appear grossly tuned to the active temperature range of the channel.

The random forest suggests that the lower eigenvalue PC modes exert the most influence on gate expansion. Of the first four PCs, the random forest found only PC2 to have a number of contacts similar to the latter 3 PCs that are predictive of the expanded gate. PC 2's strong order promoting trend, clustered in the middle of the protomer, must then be critical for the domain coupling and allosteric network reorganization that allows the lower eigenvalue mode dynamics originating from the intracellular region to communicate with the gate.

The lower eigenvalue modes necessarily display the weakest temperature response of the PCs investigated but, as a consequence, offer an explanation for the robust regulation of the different thermo-TRP activation temperatures. A tightly controlled activation mechanism producing a small ~1.5 angstrom expansion concomitant with a slight helix reorientation should naturally be encoded by the subtler trends such as PC 6 which clusters near the gate and PC7 which clusters around the IPCD, regions displaying state-dependent conformations. Once the channel is primed for activation by heat-induced contact mode evolution and network reorganization, a subtle dynamic originating from the vicinity of the IPCD regulates the final step in gate expansion.

By burying functionally critical dynamics in lower eigenvalue modes and in the middle of the temperature-sensitivity scale, activation is effectively buffered from noise; an essential feature for biomolecules designed to report on noxious stimuli. From a design standpoint, controlling function with several "layers" of modes offers nature (or protein engineers) multiple "dials" with which to precisely tune function.

Along with the detailed description of domain coupling and allosteric pathways of TRPV3 presented here, we have introduced temperature-sensitive contact analysis as a framework for investigating other heat sensitive ion channels. Further, investigation of biomolecular dynamics using these modes need not be restricted to phenomena transecting temperature, as they describe correlated interactions that conceivably exist at any temperature where the protein maintains its native fold. As we have shown here, with the right reaction coordinate, machine learning techniques can be used to map these modes to their functional roles.

Methods

Simulations

Using the Charmm GUIi's [57,58] Membrane Builder tool [59–61], we assembled our simulation system around the closed PDB 7MIJ structure[8] with which we could capture any processes that occur as it moved up through temperature. The 7mij structure is missing its disordered tails but importantly, there are no missing loops that require modeling. We formulated the membrane composition similar to the system simulated in Nadezhdin et al. [8] with the lipid models available in in Charmm-Gui as follows: 28% cholesterol, 13% phosphatidylglycerol, 22% phosphatidylcholine, 13% phosphatidylethanolamine, 4% phosphatidylinositol, 9% sphingomyelin, and 13% phosphatidylserine. The system was solvated with the TIP3P water model[62] and neutralized with sodium ions. The resulting system contained approximately 870 lipid molecules in the bilayer and 470000 atoms in total. The system was first equilibrated in several 125-500ps steps during which harmonic restraints on the protein and membrane lipids were gradually removed.

After equilibrating the fast degrees of freedom, production simulations were done with the Hamiltonian Replica Exchange Molecular Dynamics (HREMD) method across 28 effective temperatures from 300 to 420 K where exclusively protein atoms were treated with the Hamiltonian scaling factor [63–69]. The protein, membrane, and solvent were separately coupled to a Nose-Hoover thermostat at a 1ps interval and a temperature of 300K. Pressure was controlled semi-isotropically with a Parrinello-Rahman barostat at a 5ps interval and a reference pressure of 1 bar. The Particle Mesh Ewald method was used for electrostatic calculations with a 1.2nm cutoff. The HREMD simulations were run using Gromacs 2019.6 patched with Plumed 2.6.1 [63,64,67,68,70,71] on the Xsede [72] Expanse cluster using a 2fs timestep for 110 ns and replica exchanges attempted every 2ps. All contact frequency based analyses were done using the 4 protomers' identical contact pairs, effectively quadrupling the enhanced sampling time per temperature to 440ns. Convergence was determined by observing little to no change in contact frequencies among the most temperature-sensitive contacts at sensitization temperature (54 °C system) for the first two PCs (highest explained variance components) across the latter 25% of the simulation (Fig. S11)

Contacts

After removing the solvent and lipids from each of the 28 systems we calculated all of the residues' pairwise contact frequencies using GetContacts [73] which takes into account each residue's unique chemical character and assigns different cutoff distances and interaction angles defining a contact accordingly. The contact frequencies for each pairwise interaction quantify the amount of simulation time the residue pair spends in contact. Approximately 11,000 different contacts occur on each protomer (including inter-protomer contacts) with nearly half of these being extremely rare or only occurring at extreme temperature.

Principal component analysis of the averaged (see "Simulations") contact frequency data was performed with SciKit-Learn [74]. Analysis was done following the method described in Burns et al. [25]. The loading scores (eigenvector components) of the PCs were labeled with their initial variables (contact ids) and sorted according to their normalized absolute values to

find the most temperature sensitive contacts on the given PCs. The first seven PCs provided the best general picture of the channel's dynamics based on their structural clustering and on them capturing residues that correspond to observations in published literature. All of the residues with contacts occurring in the 99.85th percentile (See S3) of the first 7 PC's sorted loading scores were depicted on the structure using the contact's PC on which it had its highest overall normalized loading score. For clarity, if a residue had a contact with a loading score of .8 on PC1 and a different contact with a score of .85 on PC4, the PC4 contact was depicted. The contact frequencies were projected onto each PC and plotted as a function of temperature and smoothed via spline interpolation.

Network Analysis

The (inverse) contact frequencies were utilized as network edge weights with the NetworkX 2.8.4[75] library. The Girvan-Newman algorithm was used to deconstruct the networks into communities for the systems corresponding to 27°C and 54°C into 6 communities. The same edge weights were used with the edge-betweenness centrality algorithm and the top 86 edges from the 54°C (above sensitization) system were visualized on the structure as these were in the high, rapidly decaying region of edge-betweenness values (See Fig S6). This number was chosen also because the experimentally relevant contacts were already identified in the top third of these high centrality values.

Cartesian Coordinate PCA

We separated the trajectories into the individual subunits, concatenated them into an extended single-subunit trajectory from the 54°C simulation to extract the motions relevant to activity at enhanced temperature. The MDAnalaysis [76,77] implementation of PCA was used to calculate the principal components from the CA coordinates. For visualization, the all-atom trajectories were projected onto the PCs using the MDAnalysis method of applying a displacement vector to all the atoms in the residue corresponding to the CA atom used in the calculation of the PCs. From the frames where the structure exhibited an RMSD value in the 99th percentile, we extracted 2 frames at the endpoints of the concerted motion. Residue RMSF was calculated from the CA coordinates of these 2 frames with MDAnalaysis and colors were applied along a gradient according to each CA''s normalized RMSF (RMSF(resi)/RMSF(max)).

Gate Measurements

The trajectories were aligned so that the pore was in the same position for each Hole calculation. The MDAnalysis implementation of Hole2 [52,78] was applied to each frame of each temperature's trajectory and the minimum value from the coordinate range corresponding to the gate region was extracted.

Random Forest

The frame-by-frame contact records from 5 systems ranging in temperature from 38°C to 54°C were concatenated. These temperatures were selected as they are all within physiological activation temperatures and at the peak of the P(expanded gate) data in that temperature range and should therefore capture the contacts that are most physically relevant to the expanded

gate. Each subunit's set of contacts were separated and treated as individual samples. This effectively reduced the number of features per sample by ¾ and quadrupled the total samples.

Contacts that did not occur for identical residue pairs for all subunits were removed. To discretize the expanded and closed gate states and improve the accuracy of the model, we removed frames where the gate radius was between 0.75 and 1 angstrom.Because the number of frames with a closed gate state greatly outnumbered the frames with the expanded state (90/10 ratio), we retained only the closed state frames from the 38 °C (lowest temperature simulation used in the random forest) system which provided a more balanced data set with approximately 15,000 expanded states and 30,000 closed states. Contacts not occurring on any of the frames in this dataset were removed, reducing the number of contacts used to build the model to approximately 3,700.

We fit several models with 3-fold cross validation and an 80/20 train/test split ,varying the number of estimators between 100 to 1000, and 60 and 500 features per split. Results were reported from 2 models using 60 features each and 100 and 250 estimators respectively. The top 100 feature importances were selected for consideration as the feature importance values flatlined beyond this point (Fig S9). The contacts that were shared by both models' top 100 feature importances (83 total) were visualized on the structure and colored according to the PC on which they have their highest loading score.

Visualizations

Visualizations were produced with PyMol and the in-house scripts will be deposited in the Github upon publication of the manuscript.

Acknowledgments.

This work was supported by funds from the National Institute of General Medical Sciences with grant no. R35GM133488 (to V.V.) and grant no. R35 GM138243 (to D.P.).

1. Xu H, Ramsey IS, Kotecha SA, Moran MM, Chong JA, Lawson D, et al. TRPV3 is a calcium-permeable temperature-sensitive cation channel. Nature. 2002;418: 181–186.

2. Smith GD, Gunthorpe MJ, Kelsell RE, Hayes PD, Reilly P, Facer P, et al. TRPV3 is a temperature-sensitive vanilloid receptor-like protein. Nature. 2002;418: 186–190.

3. Peier AM, Reeve AJ, Andersson DA, Moqrich A, Earley TJ, Hergarden AC, et al. A heat-sensitive TRP channel expressed in keratinocytes. Science. 2002;296: 2046–2049.

4. Lin Z, Chen Q, Lee M, Cao X, Zhang J, Ma D, et al. Exome sequencing reveals mutations in TRPV3 as a cause of Olmsted syndrome. Am J Hum Genet. 2012;90: 558–564.

5. Jain A, Sahu RP, Goswami C. Olmsted syndrome causing point mutants of TRPV3 (G568C and G568D) show defects in intracellular Ca2+-mobilization and induce lysosomal defects. Biochem Biophys Res Commun. 2022;628: 32–39.

6. Lisa S. Martin, Emma Fraillon, Fabien P. Chevalier and Bérengère Fromy. Hot on the Trail of Skin Inflammation: Focus on TRPV1/TRPV3 Channels in Psoriasis. Available: https://www.intechopen.com/online-first/80967

7. Asakawa M, Yoshioka T, Matsutani T, Hikita I, Suzuki M, Oshima I, et al. Association of a mutation in TRPV3 with defective hair growth in rodents. J Invest Dermatol. 2006;126: 2664–2672.

8. Nadezhdin KD, Neuberger A, Trofimov YA, Krylov NA, Sinica V, Kupko N, et al. Structural mechanism of heat-induced opening of a temperature-sensitive TRP channel. Nat Struct Mol Biol. 2021;28: 564–572.

9. Zubcevic L, Borschel WF, Hsu AL, Borgnia MJ, Lee S-Y. Regulatory switch at the cytoplasmic interface controls TRPV channel gating. Elife. 2019;8. doi:10.7554/eLife.47746

10. Goretzki B, Guhl C, Tebbe F, Harder J-M, Hellmich UA. Unstructural Biology of TRP Ion Channels: The Role of Intrinsically Disordered Regions in Channel Function and Regulation. J Mol Biol. 2021;433: 166931.

11. Liu B, Qin F. Single-residue molecular switch for high-temperature dependence of vanilloid receptor TRPV3. Proc Natl Acad Sci U S A. 2017;114: 1589–1594.

12. Zubcevic L, Herzik MA Jr, Wu M, Borschel WF, Hirschi M, Song AS, et al. Conformational ensemble of the human TRPV3 ion channel. Nat Commun. 2018;9: 4773.

13. Liu B, Yao J, Zhu MX, Qin F. Hysteresis of gating underlines sensitization of TRPV3 channels. J Gen Physiol. 2011;138: 509–520.

14. Xiao R, Tang J, Wang C, Colton CK, Tian J, Zhu MX. Calcium plays a central role in the sensitization of TRPV3 channel to repetitive stimulations. J Biol Chem. 2008;283: 6162–6174.

15. Shimada H, Kusakizako T, Dung Nguyen TH, Nishizawa T, Hino T, Tominaga M, et al. The structure of lipid nanodisc-reconstituted TRPV3 reveals the gating mechanism. Nat Struct Mol Biol. 2020;27: 645–652.

16. Kasimova MA, Yazici AT, Yudin Y, Granata D, Klein ML, Rohacs T, et al. A hypothetical molecular mechanism for TRPV1 activation that invokes rotation of an S6 asparagine. J Gen Physiol. 2018;150: 1554–1566.

17. Zubcevic L, Herzik MA Jr, Chung BC, Liu Z, Lander GC, Lee S-Y. Cryo-electron microscopy structure of the TRPV2 ion channel. Nat Struct Mol Biol. 2016;23: 180–186.

18. Singh AK, McGoldrick LL, Demirkhanyan L, Leslie M, Zakharian E, Sobolevsky AI. Structural basis of temperature sensation by the TRP channel TRPV3. Nat Struct Mol Biol. 2019;26: 994–998.

19. Ladrón-de-Guevara E, Dominguez L, Rangel-Yescas GE, Fernández-Velasco DA, Torres-Larios A, Rosenbaum T, et al. The Contribution of the Ankyrin Repeat Domain of TRPV1 as a Thermal Module. Biophys J. 2020;118: 836–845.

20. Sakipov S, Sobolevsky AI, Kurnikova MG. Ion Permeation Mechanism in Epithelial Calcium Channel TRVP6. Sci Rep. 2018;8: 5715.

21. Kasimova MA, Yazici AT, Yudin Y, Granata D, Klein ML, Rohacs T, et al. A consistent picture of TRPV1 activation emerges from molecular simulations and experiments. bioRxiv. 2018. p. 310151. doi:10.1101/310151

22. Kasimova MA, Yazici A, Yudin Y, Granata D, Klein ML, Rohacs T, et al. Ion Channel Sensing: Are Fluctuations the Crux of the Matter? J Phys Chem Lett. 2018;9: 1260–1264.

23. Chugunov AO, Volynsky PE, Krylov NA, Nolde DE, Efremov RG. Temperature-sensitive gating of TRPV1 channel as probed by atomistic simulations of its trans- and juxtamembrane domains. Sci Rep. 2016;6: 33112.

24. Zheng W, Wen H. Heat activation mechanism of TRPV1: New insights from molecular dynamics simulation. Temperature (Austin). 2019;6: 120–131.

25. Burns D, Singh A, Venditti V, Potoyan DA. Temperature-sensitive contacts in disordered loops tune enzyme I activity. Proc Natl Acad Sci U S A. 2022;119: e2210537119.

26. Yao J, Liu B, Qin F. Modular thermal sensors in temperature-gated transient receptor potential (TRP) channels. Proc Natl Acad Sci U S A. 2011;108: 11109–11114.

27. Niu C, Sun X, Hu F, Tang X, Wang K. Molecular determinants for the chemical activation of the warmth-sensitive TRPV3 channel by the natural monoterpenoid carvacrol. J Biol Chem. 2022;298: 101706.

28. Singh AK, McGoldrick LL, Sobolevsky AI. Structure and gating mechanism of the transient receptor potential channel TRPV3. Nat Struct Mol Biol. 2018;25: 805–813.

29. Grandl J, Hu H, Bandell M, Bursulaya B, Schmidt M, Petrus M, et al. Pore region of TRPV3 ion channel is specifically required for heat activation. Nat Neurosci. 2008;11: 1007–1013.

30. Shi D-J, Ye S, Cao X, Zhang R, Wang K. Crystal structure of the N-terminal ankyrin repeat domain of TRPV3 reveals unique conformation of finger 3 loop critical for channel function. Protein Cell. 2013;4: 942–950.

31. Feng Q. Temperature sensing by thermal TRP channels: thermodynamic basis and molecular insights. Curr Top Membr. 2014;74: 19–50.

32. Cordero-Morales JF, Gracheva EO, Julius D. Cytoplasmic ankyrin repeats of transient receptor potential A1 (TRPA1) dictate sensitivity to thermal and chemical stimuli. Proc Natl Acad Sci U S A. 2011;108: E1184–91.

33. Latorre R, Brauchi S, Orta G, Zaelzer C, Vargas G. ThermoTRP channels as modular proteins with allosteric gating. Cell Calcium. 2007;42: 427–438.

34. Vlachová V, Teisinger J, Susánková K, Lyfenko A, Ettrich R, Vyklický L. Functional role of C-terminal cytoplasmic tail of rat vanilloid receptor 1. J Neurosci. 2003;23: 1340–1350.

35. Jara-Oseguera A, Islas LD. The role of allosteric coupling on thermal activation of thermo-TRP channels. Biophys J. 2013;104: 2160–2169.

36. Jara-Oseguera A, Huffer KE, Swartz KJ. The ion selectivity filter is not an activation gate in TRPV1-3 channels. Elife. 2019;8. doi:10.7554/eLife.51212

37. Jabba S, Goyal R, Sosa-Pagán JO, Moldenhauer H, Wu J, Kalmeta B, et al. Directionality of temperature activation in mouse TRPA1 ion channel can be inverted by single-point mutations in ankyrin repeat six. Neuron. 2014;82: 1017–1031.

38. Zhang K, Julius D, Cheng Y. Structural snapshots of TRPV1 reveal mechanism of polymodal functionality. Cell. 2021;184: 5138–5150.e12.

39. Di Paola L, Mei G, Di Venere A, Giuliani A. Disclosing Allostery Through Protein Contact Networks. Methods Mol Biol. 2021;2253: 7–20.

40. Foutch D, Pham B, Shen T. Protein conformational switch discerned via network centrality properties. Comput Struct Biotechnol J. 2021;19: 3599–3608.

41. Vishveshwara S, Brinda KV, Kannan N. PROTEIN STRUCTURE: INSIGHTS FROM GRAPH THEORY. J Theor Comput Chem. 2002;01: 187–211.

42. Di Paola L, De Ruvo M, Paci P, Santoni D, Giuliani A. Protein contact networks: an emerging paradigm in chemistry. Chem Rev. 2013;113: 1598–1613.

43. De Ruvo M, Giuliani A, Paci P, Santoni D, Di Paola L. Shedding light on protein–ligand binding by graph theory: The topological nature of allostery. Biophys Chem. 2012;165-166: 21–29.

44. Girvan M, Newman MEJ. Community structure in social and biological networks. Proc Natl Acad Sci U S A. 2002;99: 7821–7826.

45. Freeman LC. A Set of Measures of Centrality Based on Betweenness. Sociometry. 1977;40: 35–41.

46. Neuberger A, Nadezhdin KD, Zakharian E, Sobolevsky AI. Structural mechanism of TRPV3 channel inhibition by the plant-derived coumarin osthole. EMBO Rep. 2021;22: e53233.

47. Lejla Zubcevic S-YL. The role of pi-helices in TRP channel gating. Current Opinion in Structural Biology. 2019;58: 314–323.

48. Myers BR, Bohlen CJ, Julius D. A yeast genetic screen reveals a critical role for the pore helix domain in TRP channel gating. Neuron. 2008;58: 362–373.

49. Wang Y, Tan L, Jiao K, Xue C, Tang Q, Jiang S, et al. Scutellarein attenuates atopic dermatitis by selectively inhibiting transient receptor potential vanilloid 3 channels. Br J Pharmacol. 2022. doi:10.1111/bph.15913

50. Hu H, Grandl J, Bandell M, Petrus M, Patapoutian A. Two amino acid residues determine 2-APB sensitivity of the ion channels TRPV3 and TRPV4. Proc Natl Acad Sci U S A. 2009;106: 1626–1631.

51. Liu B, Qin F. Identification of a helix-turn-helix motif for high temperature dependence of vanilloid receptor TRPV2. J Physiol. 2021;599: 4831–4844.

52. Smart OS, Neduvelil JG, Wang X, Wallace BA, Sansom MS. HOLE: a program for the analysis of the pore dimensions of ion channel structural models. J Mol Graph. 1996;14: 354–60, 376.

53. Shannon RD. Revised effective ionic radii and systematic studies of interatomic distances in halides and chalcogenides. Acta Crystallogr A. 1976;32: 751–767.

54. Zhang W, Cheng LE, Kittelmann M, Li J, Petkovic M, Cheng T, et al. Ankyrin Repeats

Convey Force to Gate the NOMPC Mechanotransduction Channel. Cell. 2015;162: 1391–1403.

55. Ito E, Ikemoto Y, Yoshioka T. Thermodynamic implications of high Q 10 of thermo-TRP channels in living cells. Biophysics . 2015;11: 33–38.

56. Clapham DE, Miller C. A thermodynamic framework for understanding temperature sensing by transient receptor potential (TRP) channels. Proc Natl Acad Sci U S A. 2011;108: 19492–19497.

57. Jo S, Kim T, Iyer VG, Im W. CHARMM-GUI: a web-based graphical user interface for CHARMM. J Comput Chem. 2008;29: 1859–1865.

58. Lee J, Cheng X, Swails JM, Yeom MS, Eastman PK, Lemkul JA, et al. CHARMM-GUI Input Generator for NAMD, GROMACS, AMBER, OpenMM, and CHARMM/OpenMM Simulations Using the CHARMM36 Additive Force Field. J Chem Theory Comput. 2016;12: 405–413.

59. Jo S, Lim JB, Klauda JB, Im W. CHARMM-GUI Membrane Builder for mixed bilayers and its application to yeast membranes. Biophys J. 2009;97: 50–58.

60. Jo S, Kim T, Im W. Automated builder and database of protein/membrane complexes for molecular dynamics simulations. PLoS One. 2007;2: e880.

61. Wu EL, Cheng X, Jo S, Rui H, Song KC, Dávila-Contreras EM, et al. CHARMM-GUI*Membrane Builder*toward realistic biological membrane simulations. Journal of Computational Chemistry. 2014. pp. 1997–2004. doi:10.1002/jcc.23702

62. Mark P, Nilsson L. Structure and Dynamics of the TIP3P, SPC, and SPC/E Water Models at 298 K. J Phys Chem A. 2001;105: 9954–9960.

63. Tribello GA, Bonomi M, Branduardi D, Camilloni C, Bussi G. PLUMED 2: New feathers for an old bird. Comput Phys Commun. 2014;185: 604–613.

64. Bussi G, Tribello GA. Analyzing and Biasing Simulations with PLUMED. Methods Mol Biol. 2019;2022: 529–578.

65. Fukunishi H, Watanabe O, Takada S. On the Hamiltonian replica exchange method for efficient sampling of biomolecular systems: Application to protein structure prediction. J Chem Phys. 2002;116: 9058–9067.

66. Stirnemann G, Sterpone F. Recovering Protein Thermal Stability Using All-Atom Hamiltonian Replica-Exchange Simulations in Explicit Solvent. J Chem Theory Comput. 2015;11: 5573–5577.

67. Berendsen HJC, van der Spoel D, van Drunen R. GROMACS: A message-passing parallel molecular dynamics implementation. Comput Phys Commun. 1995;91: 43–56.

68. Van Der Spoel D, Lindahl E, Hess B, Groenhof G, Mark AE, Berendsen HJC. GROMACS: fast, flexible, and free. J Comput Chem. 2005;26: 1701–1718.

69. Abraham MJ, Murtola T, Schulz R, Páll S, Smith JC, Hess B, et al. GROMACS: High performance molecular simulations through multi-level parallelism from laptops to supercomputers. SoftwareX. 2015;1-2: 19–25.

70. Pronk S, Páll S, Schulz R, Larsson P, Bjelkmar P, Apostolov R, et al. GROMACS 4.5: a high-throughput and highly parallel open source molecular simulation toolkit. Bioinformatics. 2013;29: 845–854.

71. Páll S, Abraham MJ, Kutzner C, Hess B, Lindahl E. Tackling Exascale Software Challenges in Molecular Dynamics Simulations with GROMACS. Solving Software Challenges for Exascale. Springer International Publishing; 2015. pp. 3–27.

72. Towns J, Cockerill T, Dahan M, Foster I, Gaither K, Grimshaw A, et al. XSEDE: Accelerating Scientific Discovery. Computing in Science & Engineering. 2014. pp. 62–74. doi:10.1109/mcse.2014.80

73. getcontacts: Library for computing dynamic non-covalent contact networks in proteins throughout MD Simulation. Github; Available: https://github.com/getcontacts/getcontacts

74. Pedregosa, Varoquaux, Gramfort. Scikit-learn: Machine learning in Python. the Journal of machine. Available: https://www.jmlr.org/papers/volume12/pedregosa11a/pedregosa11a.pdf?ref=https://githubhelp.com

75. Hagberg A, Swart P, S Chult D. Exploring network structure, dynamics, and function using networkx. Los Alamos National Lab. (LANL), Los Alamos, NM (United States); 2008 Jan. Report No.: LA-UR-08-05495; LA-UR-08-5495. Available: https://www.osti.gov/biblio/960616

76. Michaud-Agrawal N, Denning EJ, Woolf TB, Beckstein O. MDAnalysis: a toolkit for the analysis of molecular dynamics simulations. J Comput Chem. 2011;32: 2319–2327.

77. Gowers RJ, Linke M, Barnoud J, Reddy TJE, Melo MN, Seyler SL, et al. MDAnalysis: a Python package for the rapid analysis of molecular dynamics simulations. Los Alamos National Lab.(LANL), Los Alamos, NM (United States); 2019. Available: https://conference.scipy.org/proceedings/scipy2016/pdfs/oliver_beckstein.pdf

78. Smart OS, Goodfellow JM, Wallace BA. The pore dimensions of gramicidin A. Biophys J. 1993;65: 2455–2460.